Journal of African Earth Sciences 194 (2022) 104612

Contents lists available at ScienceDirect

Journal of African Earth Sciences

journal homepage: www.elsevier.com/locate/jafrearsci

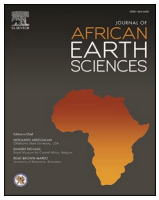

Rigorous evaluation of global geopotential models for geoid modelling: A case study in Kenya

Chivatsi Jonathan Nyoka [a,**], Ami Hassan Md Din [a,b,*], Muhammad Faiz Pa'suya [c], Abdullah Hisam Omar [d]

[a] Geospatial Imaging and Information Research Group (GI2RG), Faculty of Built Environment and Surveying, Universiti Teknologi Malaysia, 81310, Skudai, Johor, Malaysia
[b] Geoscience and Digital Earth Centre (INSTeG), Faculty of Built Environment and Surveying, Universiti Teknologi Malaysia, 81310, Skudai, Johor, Malaysia
[c] Environment and Climate Change Research Group (ECCG) Faculty of Architecture, Planning & Surveying, Universiti Teknologi MARA, Perlis, Arau Campus, 02600, Arau, Perlis, Malaysia
[d] Geomatics Innovation Research Group (GnG), Faculty of Built Environment and Surveying, Universiti Teknologi Malaysia, 81310, Skudai, Johor, Malaysia

ARTICLE INFO

Keywords:
Global geopotential model
Spectral analysis
Geoid modelling
Zero-degree terms
Permanent tide
Gravimetric geoid

ABSTRACT

Developing a gravimetric geoid model requires gravity data covering the whole surface of the earth. In practice, terrestrial data within a spherical cap is used, causing a truncation error, which may be minimised if the terrestrial data is combined with a Global Geopotential Model (GGM). The choice of a GGM that fits the observed terrestrial data best, determines the accuracy of a gravimetric geoid solution. In this study, the most recent and high-resolution GGMs are selected and compared, both geometrically and spectrally with a view to selecting an optimum GGM for future geoid modelling in Kenya. In the first step, thirty-one GGMs are evaluated using 55 GNSS-levelled points scattered over 4 regions and gravity data distributed over the entire territory of Kenya. In the second step, some of the best performing GGMs are further compared using the spectral information contained in their spherical harmonic coefficients. After removal of systematic errors, the EGM2008 model showed some advantage over other GGMs with a standard deviation of 40.89 cm. Other high-resolution geoid models perform well in terms of recovering geoid heights in Kenya with a standard deviation of $<$42 cm. In terms of residual gravity anomalies, the EIGEN-6C4 model showed the best fit with a standard deviation of 6.892 mGal. In the spectral analysis, the XGM2016 provided the best results among the models evaluated. Based on the overall performance in all areas of evaluation, the SGG-UGM-1 and SGG-UGM-2 were considered best for geoid modelling in Kenya.

1. Introduction

To create a gravimetric geoid model, the Stokes integral equations are extensively employed to derive geoidal undulations from terrestrial gravity measurements at points on or above the earth's surface. These formulae require gravity data covering the whole earth, but, in practice, discrete gravity data is available only within a spherical cap. A truncation error is caused by the lack of gravity data, which can be reduced by merging terrestrial data with a global geopotential model (GGM). According to Kearsley and Holloway (1989), a GGM's capacity to retrieve geoid heights varies greatly depending on the points' position and the GGM's maximum degree n_{max}. For optimal gravimetric geoid determination, a GGM that fits the local gravity field in terms of observed gravity field functionals (geoid undulations, free air anomalies, etc.) must be adopted, since this decreases the impact of the inherent assumptions and approximations in the Stokes formulas. This can be accomplished by comparing gravity field functionals derived from GGMs with those obtained from GNSS-leveling and terrestrial gravity data.

In Kenya, the task of determining the geopotential model that best represents the local gravity field has yet to be resolved. Only one geoid model has been determined so far, that is unique to the country. The

* Corresponding author. Geospatial Imaging and Information Research Group (GI2RG), Faculty of Built Environment and Surveying, Universiti Teknologi Malaysia, 81310, Skudai, Johor, Malaysia.
** Corresponding author.
E-mail addresses: jnchivatsi@graduate.utm.my (C.J. Nyoka), amihassan@utm.my (A.H.M. Din).

https://doi.org/10.1016/j.jafrearsci.2022.104612
Received 21 November 2021; Received in revised form 1 June 2022; Accepted 4 June 2022
Available online 9 June 2022

Table 1
Earth Gravity models used.

S/N	Model	Year	Degree	Data
1	SGG-UGM-2	2020	2190	A, EGM 2008, Grace (GOCE)
2	XGM 2019e_2159	2019	2190	A, G, S (GOCO06s), T
3	XGM 2019e	2019	5540	A, G, S (GOCO06s), T
4	XGM2019	2019	760	A, G, S (GOCO06s), T
5	ITSG-Grace2018s	2019	200	S (Grace)
6	GOCO06s	2019	300	S
7	GO_CONS_GCF_2_TIM_R6	2019	300	S (Goce)
8	GO_CONS_GCF_2_DIR_R6	2019	300	S
9	IGGT_R1C	2018	240	G, S, S (Grace)
10	Tongji-Grace02k	2018	180	S (Grace)
11	SGG-UGM-1	2018	2159	EGM 2008, S (Goce)
12	GOSG01S	2018	220	S (Goce)
13	IGGT_R1	2017	240	S (Goce)
14	IfE_GOCE05s	2017	250	S
15	GO_CONS_GCF_2_SPW_R5	2017	330	S (Goce)
16	XGM2016	2017	719	A, G, S (GOCO05s)
17	Tongji-Grace02s	2017	180	S (Grace)
18	NULP-02s	2017	250	S (Goce)
19	EIGEN-6C4	2014	2190	A, G, S (Goce, Grace, Lageos)
20	GO_CONS_GCF_2_DIR_R5	2014	300	S (Goce, Grace, Lageos)
21	GO_CONS_GCF_2_TIM_R4	2013	250	S (Goce)
22	GO_CONS_GCF_2_TIM_R3	2011	250	S (Goce)
23	GO_CONS_GCF_2_TIM_R2	2011	250	S (Goce)
24	GOCO02s	2011	250	S (Goce, Grace)
25	EGM2008	2008	2190	A, G, S (Grace)
26	EIGEN-GL04C	2006	360	A, G, S (Grace, Lageos)
27	eigen-cg03c	2005	360	A, G, S (Champ, Grace)
28	EIGEN-CHAMP03S	2004	140	S(Champ)
29	EGM96	1996	360	A, EGM96S, G
30	EIGEN-2	2003	140	S(Champ)
31	GEM10b	1978	36	A, GEM10

Notes: Data: S = Satellite tracking data, G = Gravity data, A = Altimetry data.
Source: ICGEM page: icgem.gfz-postdam.de/tom_longtime

GEM10B geopotential model was used to create this model, with coefficients up to the maximum degree and order 36 (Gachari and Olliver, 1986). Since then, high-quality GGMs have been produced using measurements or combination of measurements collected from terrestrial and advanced satellite missions, with a spatial resolution of 9 km and a maximum degree of 2190 (Ince et al., 2019). Such measurements are in terms of satellite orbital perturbations computed from GNSS measurements, satellite laser ranging (SLR) observations, range rate measurements between two satellites using microwave and laser, and gravity gradients and non-gravitational accelerations measured using space-borne sensors (Ince et al., 2019).

Few studies have been made to assess the suitability of GGMs over Kenya. In Odera (2016), the suitability of Earth Gravitational Model 2008 (EGM2008) was assessed within Nairobi County and its metropolitan area, using GPS-levelling geoid undulations and free-air gravity anomalies. In Odera (2020), an assessment was done of high-resolution GGMs (EIGEN-6C4, SGG-UGM-1, EGM 2008, and GECO) using observed free-air gravity anomalies distributed all over Kenya and GPS-levelling points within Nairobi county. In both previous studies, only 18 GNSS-levelling points within the Nairobi metropolitan area were used.

Global geopotential models are available from the International Centre for Global Earth Models (ICGEM). ICGEM is a service that provides scientists with a collection of global gravity field models that are either static or temporal. Furthermore, through its website (http://icgem.gfzpotsdam.de/ICGEM/-ICGEM.html), ICGEM has developed and operated an interactive calculation and visualization service for computing gravity field functionals on user-defined grids or points, where about 180 GGMs are available. The website has a summary of the datasets used in the computation of the models, where A represents altimetry, S is for satellite (e.g., GRACE, GOCE, LAGEOS), G for terrestrial, ship-borne and/or airborne measurements, and T for topography. Therefore, the precision, as well as the maximum degree of the GGMs, vary significantly. With the number of geopotential models growing every year, it will be difficult for the user to select the optimum model for their regional modelling without testing each model.

Table 2
Statistics for height and gravity data used (Units in mGal for anomalies and metres otherwise).

	Min	Max	Mean	Std Dev.
Ellipsoidal height (h)	−24.546	−4.327	−11.858	6.000
Orthometric height (H)	4.240	2144.200	1108.005	805.880
Observed undulations (h-H)	−29.643	−28.131	−28.812	0.354
Observed Free air Anomalies	−126.980	1094.186	76.835	231.168

The aim of this study is to evaluate the performance of the most recent and high-resolution GGMs available at ICGEM for future geoid modelling in Kenya. A rigorous scheme is used by first filtering the models using GNSS geoid undulations and observed gravity anomalies, then analyzing the spectral information contained in the GGMs to obtain the optimum model(s) for future geoid modelling in Kenya.

2. Data used

The dataset used in the present study include the most recent and highest resolution GGMs, GNSS-levelled points and point free-air gravity anomalies. The dataset is described in the following subsections.

2.1. Global geopotential models

A total of 31 GGMs, which are either greater than 360 by degree or were developed in the last ten years, were selected for the study. The GGMs span a wide range of models with various input data combinations (e.g., altimetry data, satellite tracking data and, terrestrial gravity data), as well as diversity in degree and order. Some bias is also made towards models with a proven track record, having been used in other parts of the world, especially in the vicinity of the study area. Even though they are older than the other GGMs, the EGM96 and EGM2008 models have been included in the study, both for historical reasons and for the fact that they have never been utilized for gravimetric geoid modelling in Kenya. The GEM10B model, having been used in Kenya as previously mentioned, was included in the study for obvious reasons. The spherical harmonic coefficient files of the GGMs were downloaded from the ICGEM website, and their specifications are shown in Table 1.

2.2. GNSS-levelled points

The vertical datum in Kenya is realized by a network of spirit-levelled points referred to a tide gauge, constructed within the Kilindini old port, at the coastal city of Mombasa in 1931. The mean sea level or tidal observations were made for a period of one year, followed by the first geodetic levelling exercise, which began in 1949 with the construction of benchmarks (Odera, 2016). The actual precise levelling was carried out between 1950 and 1958. The levelling was done along the railway line from Mombasa through Nairobi and joined the Uganda levelling network at Tororo and Buteba. For more information on the Kenyan vertical control network, one may refer to, e.g. Odera (2016). A total of 78 GNSS-levelling benchmarks from different parts of Kenya, namely, coastal, central and western parts, were used to evaluate the GGMs. The Directorate of Surveys of Kenya made GNSS observations (comprising of latitude, longitude and ellipsoidal heights) on these benchmarks, to enhance the security of tenure along riparian areas (personal communication with Director of Surveys). Table 2 shows the statistics of the data points. As seen in the table, the orthometric height varies from 4m to 2144m, suggesting a vast variance in Kenya's topography.

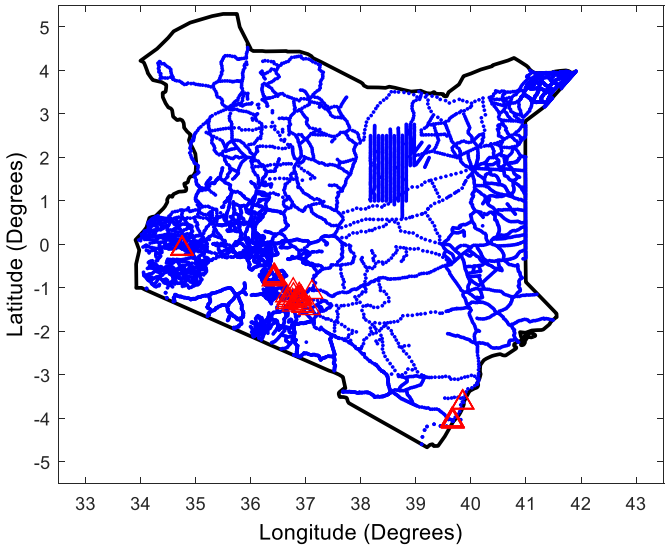

Fig. 1. Location of data points; blue dots represent the gravity stations, while the red triangles represent the GNSS-Levelled benchmarks.

Even though the data has a wide range of the Kenyan topography, it may not completely represent the whole country. However, the dataset can be used to evaluate and select a suitable GGM for geoid modelling in Kenya. GNSS observations on the benchmarks is an ongoing exercise by the Department of Surveys in Kenya, and results of such an exercise will be used to validate any future geoid models. Fig. 1 shows the positions of the gravity and GNSS/levelling points used in the current study.

2.3. Gravity data

In Kenya, gravity data comprises of gravity accelerations and Bouguer anomaly maps on land and ocean surface. According to Searle (1970), gravity observations began around 1899 and continued up to 1967. In Swain and Khan (1978), a detailed catalogue of terrestrial gravity data and resulting Bouguer anomaly maps for republic of Kenya is presented. Various companies and organizations/institutions collected the data, e.g., Leicester University, Overseas Geological Surveys, Newcastle University, British Petroleum, Burmah Oil Trading, United Nations Geothermal Project and Chevron Overseas Petroleum. A majority of the Gravity observations were made with a LaCoste & Romberg gravimeter and were based on the IGSN71 datum, having been referred to the Nairobi pendulum station. An estimated accuracy of between ±1 to ±10 gu, which translates to ±0.1 to ±1 mGal was posted for the gravity data (Odera, 2016). Unfortunately, gravity data sets recorded by petroleum corporations after 1975 are scanty and secluded in both distribution and format, besides being not accessible for this study. If available, these gravity measurements will increase the precision of geoid modeling and other geoscience applications in the country. This study used gravity acceleration data from the Bureau Gravimetrique International (BGI).

3. Method

A global geopotential model is essentially a collection of dimensionless, fully normalized spherical harmonic coefficients $\overline{C}nm$ and $\overline{S}nm$ with their errors δCnm and δSnm that can be used to simulate the earth's gravity field. These coefficients are calculated using satellite data or a combination of satellite and terrestrial gravity data (Rapp, 1974). The coefficients can be used to calculate geoid undulations, height anomalies, gravity anomalies, gravity disturbances and vertical deflections, as well as other gravity field functionals implied by the corresponding GGMs. In evaluating the suitability of GGMs for a particular region, such functionals are compared with observed quantities.

The evaluation of the selected GGMs may be carried out either internally or externally. The internal evaluation is global in nature, in the sense that it compares the spectral information of the GGMs as derived from their spherical harmonics, and the results are applicable to all parts of the world. This information includes the signal power and the formal geoid errors of the GGMs. On the other hand, external validation uses statistical analysis of the differences of the various functionals of the disturbing potential between those observed and those synthesized from the GGM. In this study, only geoid undulations and free air anomalies are used because other observed data such as gravity disturbances, vertical deflections and vertical gradients, were not available.

3.1. Synthesis of gravity field functionals from GGMs

The disturbing potential, T with respect to a point P in space may be given by the expansion (Heiskanen and Moritz, 1967; Torge, 2001; Ågren, 2004):

$$T(P) = \sum_{n=2}^{\infty} \left(\frac{R}{r_p}\right)^{n+1} T_n(P) \tag{1}$$

where R denotes the mean Earth radius, r_P is the distance of P from the origin, and T_n are the surface spherical harmonics of T given by (Heiskanen and Moritz, 1967; Torge, 2001; Ågren, 2004):

$$T_n = \frac{GM}{r} \sum_{m=0}^{n} [\overline{C}_{nm} \cos(m\lambda) + \overline{S}_{nm} \sin(m\lambda)] P_{nm} \cos(\theta) \tag{2}$$

in which GM is the geocentric gravitational constant, a is a scaling parameter associated with the GGM, $\overline{C}_{nm}$ and $\overline{S}_{nm}$ are the fully normalized spherical harmonic coefficients , P_{nm} are the fully normalized associated Legendre functions of degree n and order m, (φ, λ) are spherical polar coordinates of point P and $\theta = 90 - \varphi$ is the co-latitude of the point. The coefficients $\overline{C}_{nm}$ (n *is even and* $m = 0$) are referred to an ellipsoid of a given flattening.

Geoid undulations may be obtained by combining equation (2) with the Brun's equation to obtain (Heiskanen and Moritz, 1967; Gachari and Olliver, 1986; Torge, 2001; Ågren, 2004; Sideris, 2011):

$$N_{ggm} = N_0 + \frac{GM}{\gamma r} \sum_{n=2}^{n_{max}} \left(\frac{a}{r}\right)^n \sum_{m=0}^{n} [\overline{C}_{nm} Cos(m\lambda) + \overline{S}_{nm} Sin(m\lambda)] P_{nm} Sin(\varphi) \tag{3}$$

where r, λ, φ are the coordinates of the computation point reduced to the geoid, n_{max} is the maximum degree of the geopotential model, and other variables are as previously defined.

Gravity anomalies may also be synthesized from the spherical harmonic coefficients using (Heiskanen and Moritz, 1967; Gachari and Olliver, 1986; Torge, 2001; Ågren, 2004; Sideris, 2011):

$$\Delta g_{ggm} = \Delta g_0 + \frac{GM}{r^2} \sum_{n=2}^{nmax} \left(\frac{a}{r}\right)^n (n-1) \sum_{m=0}^{n} [\overline{C}_{nm} Cos(m\lambda) + \overline{S}_{nm} Sin(m\lambda)] P_{nm} Sin(\varphi) \tag{4}$$

where variables are as previously defined.

3.2. Zero-degree terms

In equations (3) and (4), the terms N_0 and Δg_0 are components of the zero-degree terms for geoid undulations and gravity anomalies, with respect to the reference normal ellipsoid, respectively. They account for the differences in the masses and potential between the geopotential model used and the reference ellipsoid and enable the geoid undulation and gravity anomalies to be referenced to a specific equipotential surface with W_0 and GM_E values. They may be determined from the formulae (Heiskanen and Moritz, 1967; Kirby and Featherstone, 1997):

Table 3
Signal factors of some gravity functionals (Ustun and Abbak, 2010).

Gravity functional	Symbol	Factor, k	unit
signal	c	1	$unit-less$
Disturbing potential	T	$\frac{GM}{R}$	m^2s^{-2}
Geoid height	N	R	m
Gravity anomaly	Δg	$\frac{GM}{R^2}(n-1)10^5$	$mgal$
Gravity disturbance	δg	$\frac{GM}{R^2}(n+1)10^5$	$mgal$
Vertical deflection	θ	$180\times\frac{3600}{\pi}$	$degree-sec$
Vertical gradient	δg_r	$\frac{GM}{R^3}(n+1)(n+2)10^8$	$Mgal\ km^{-1}$

$$N_0 = \frac{GM - GM_E}{R\gamma} - \frac{W_0 - U_0}{\gamma} \tag{5}$$

$$\Delta g_0 = \frac{GM_E - GM_0}{R^2} - \frac{2(W_0 - U_{0)}}{R} \tag{6}$$

where the parameters GM_E and U_0 correspond to the Somigliana-Pizzeti normal gravity field produced by the normal ellipsoid (Moritz, 1992), and other parameters are as previously defined.

3.3. Permanent tide

Most of the 31 GGMs used in the study are in the tide free system. A few, including 8 of the most recent ones, are in the zero-tide system. In terms of spherical harmonic coefficients, only the C_{20} coefficient is affected by the permanent tide. To ensure an unbiased evaluation of the models, the C_{20} coefficients of all the GGMs may be transformed into one system using the relation (Rapp et al., 1991; Zhang et al., 2020):

$$C^{T-F}{}_{20} = C^{Z-T}{}_{20} + 3.1108\times10^{-8}\times\frac{0.3}{\sqrt{5}}$$

where $C^{T-F}{}_{20}$ and $C^{Z-T}{}_{20}$ are the harmonic coefficients under the tide-free and zero-tide systems, respectively.

3.4. Comparison of spectral information of GGMs

3.4.1. Degree variances and error degree variances

Using the spherical harmonic coefficients, the signal and error degree variances of the disturbing potential may be computed from (Ustun and Abbak, 2010; Tsoulis et al., 2011):

$$c_n = k^2\sum_{m=0}^{n}\left(\overline{C}_{nm}{}^2 + \overline{S}_{nm}{}^2\right) \tag{7}$$

And the error degree variances by (Ustun and Abbak, 2010; Tsoulis et al., 2011):

$$\delta c_n = k^2\sum_{m=0}^{n}\left(\delta\overline{C}_{nm}{}^2 + \delta\overline{S}_{nm}{}^2\right) \tag{8}$$

If the appropriate eigen value, k is inserted in equations (7) and (8) all functionals of the gravity field may be computed. The factors of k corresponding to the various functionals of the disturbing potential are given in Table 3.

The signal degree variance signifies the amount of signal power implied by all the coefficients within a specific degree and is commonly referred to as the power spectrum (Ustun and Abbak, 2010; Tsoulis et al., 2011). The error degree variance, on the other hand, is an expression of how much signal power error of a given anomalous quantity exists for all the coefficients of a specific degree. The variation of power spectra with the degree may therefore be used to describe the rate of decay of the anomalous signal as the degree increases.

Table 4
Global degree anomaly variances (Rapp, 1973; Tscherning and Rapp, 1974).

Model	Formulae
Kaula (1966)	$\sqrt{\sum_{n=Nmax+1}\sigma_N{}^2} = \frac{64}{Nmax}$
Tscherning and Rapp (1974)	$\sigma^2{}_{n>3} = \frac{A(n-1)}{(n-2)(n+B)}$ where A = 425, B = 24 $\sigma^2{}_{n==0,1} = 0$ $\sigma^2{}_{n==2} = 754$
Rapp (1973)	$\sigma^2{}_{n>3} = \frac{A(n-1)}{(n-2)(n+B+C*n^2)}$ where $A = 246.5556$, $B = 12.6755$, *and* $C = 0.000657$

3.4.2. Root mean square error

The root mean square (RMS) by degree of gravity functionals may be obtained by taking the square root of the degree variances (Rapp, 1973; Ustun and Abbak, 2010; Tsoulis et al., 2011):

$$c^{rms}{}_n = k\sqrt{\frac{\sum_{m=0}^{n}\left(\overline{C}_{nm}{}^2 + \overline{S}_{nm}{}^2\right)}{n^2}} \tag{9}$$

While the overall RMS may be obtained from (Ustun and Abbak, 2010; Tsoulis et al., 2011):

$$\sigma_T = \left(\sum_{n=2}^{\infty} c^{rms}{}_n\right)^{\frac{1}{2}} \tag{10}$$

In the current study, the root mean squares of geoidal undulations and gravity anomalies were estimated by the wavelength of the selected geopotential models. Four wavelength types were selected as defined in Rapp (1973):

1. Long wavelengths: gravity field functional information contained from degrees n = 2 to n = 10, equivalent to a linear half-wavelength of 2000 km and more.
2. Intermediate wavelength: for the gravity field functional information contained in degrees n = 11 to n = 100 equivalent to a linear half-wavelength of 200–2000 km.
3. Short wavelength: gravity field functional information contained in degrees n = 101 to n = 1000 equivalent to a linear half-wavelength of 20–200 km.
4. Very short wavelength: gravity field functional information contained in degrees 1001 to ∞ equivalent to a linear half-wavelength less than 20 km.

In total, the RMS of the point geoid gravity functionals may be expressed in terms of the wavelength components using (Rapp, 1973):

$$\sigma_T = \sigma_{2,10}{}^2 + \sigma_{11,100}{}^2 + \sigma_{101,1000}{}^2 + \sigma_{>1000}{}^{2\frac{1}{2}} \tag{11}$$

3.4.3. Signal to noise ratio

The signal-to-noise (SNR) ratio may be computed both cumulatively or by degree. The signal by degree may be obtained from (Tziavos et al., 2015)

$$S_{nr} = \frac{c_n}{\delta c_n} \tag{12}$$

3.4.4. Omission and commission errors

Global geopotential models are subject to two types of data errors; the commission errors, which involve the noise in the observations that were used to calculate the GGM spherical harmonic coefficients, and the omission error, arising due to limitations of the GGMs not to include the frequencies beyond the maximum degree (Wang, 2012). Omission errors may be estimated from global degree variances using the equation (Wang, 2012):

$$err = \sum_{n=Nmax+1}^{\infty} {c_n}^2 \tag{13a}$$

A certain higher degree, e.g., 10,000 (Tscherning and Rapp,1974), is used in practice. The global degree anomaly variances models commonly used are shown in Table 4.

3.5. Comparison with GNSS-levelled heights

Observed Geoid heights, N_{gnss} can be calculated from the GNSS-measured ellipsoidal heights, h and spirit-levelled orthometric heights, H at benchmarks, using the famous equation (Ismail et al., 2018):

$$N_{gnss} = h - H \tag{13b}$$

These heights are independent of the gravimetric-determined geoid heights and, therefore, ideal for validating geoid models' precision, including GGMs. The model-derived geoid undulations implied by the GGMS may be obtained from equation (3). To assess the suitability of the different GGMs, the differences or bias for each GGM were calculated for statistical analysis using the following equation (Ismail et al., 2018):

$$\delta N = N_{gnss} - N_{ggm} \tag{14}$$

where N_{ggm} is the geoid height obtained from the GGM.

The basic statistical indicators, such as the minimum, maximum, mean and standard deviation, were then obtained. To minimize the effect of systematic errors and datum inconsistencies (Kotsakis and Sideris, 1999; Sjöberg and Bagherbandi, 2017) between the geoid undulations obtained from GNSS-levelling and GGMs, various parametric models were fitted into the observations using the equation (Ismail et al., 2018):

$$\delta N = Ax \tag{15}$$

where x is a vector of the unknown parameters, and A is the design matrix corresponding to the known coefficients of a pre-selected parametric model. In this study, three, four, five and seven parametric models were used, respectively as follow (Goyal et al., 2018):

Three parameters:

$$A = [\,cos\varphi cos\lambda \quad cos\varphi sin\lambda \quad sin\varphi\,] \tag{16}$$

Four parameters:

$$A = [\,1 \quad cos\varphi cos\lambda \quad cos\varphi sin\lambda \quad sin\varphi\,] \tag{17}$$

Five parameters:

$$A = [\,1 \quad cos\varphi cos\lambda \quad cos\varphi sin\lambda \quad sin\varphi \quad sin^2\varphi\,] \tag{18}$$

Seven parameters:

$$A = \left[cos\varphi cos\lambda \quad cos\varphi sin\lambda \quad sin\varphi \quad \frac{cos\varphi sin\varphi sin\lambda}{w} \quad \frac{cos\varphi sin\varphi cos\lambda}{w} \quad \frac{1 - f^2 sin^2\varphi}{w} \quad \frac{sin^2\varphi}{w} \right] \tag{19}$$

where f and e are the flattening and first eccentricity, respectively of the reference ellipsoid and w is given by. $\sqrt{1 - e2sin2\varphi}$.

The unweighted least-squares adjustment was used since there was no information on the accuracy of both the observed and the synthesized geoid undulations. The solution to the least-squares adjustment was of the form (Setan and Singh, 2001; Ghilani and Wolf, 2006):

$$X = \left(A^T PA\right)^{-1}\left(A^T PL\right) \tag{20}$$

$$v = AX - L \tag{21}$$

Table 5
Statistics for geoid undulations and gravity free-air anomalies used at 7456 points (Units in metres for undulations and mGal for gravity anomalies).

	Min	Max	Mean	Std Dev.
Observed undulations (h-H)	−29.643	−12.700	−20.137	6.231
Observed Free air Anomalies	−22.344	20.147	−4.363	11.424

$$\sigma = \sqrt{\frac{v^T V}{r}} \tag{22}$$

where $L = \delta N$ is the vector of observations, A is the design matrix, v the vector of residuals, σ the standard deviation, $r = n - m$ the degrees of freedom, n the number of evaluation points and m the number of unknown parameters in terms of the parametric model.

3.6. Comparison with gravity anomalies

The assessment was carried out by first synthesizing free-air gravity anomalies from GGMs and comparing them to observed free-air gravity anomalies using equation (4). Without taking into account the atmospheric influence, the observed free-air gravity anomaly, Δg_{fa} at a point is given by (McCubbine et al., 2018):

$$\Delta g_{fa} = g_{obs} - \delta g_{fa} - \gamma_{ell} \tag{23}$$

where g_{obs} is the observed gravity and δg_{fa}, the free air reduction, is computed using the following equation (Marotta and Vidotti, 2017b):

$$\delta g_{fa} = (2\gamma\_e) \Big/ a\left(1 + f + m - 2fsin^2\varphi\right)H - \frac{3\gamma_e}{a^2}H^2 \tag{24}$$

The normal gravity on the ellipsoid, which is a function of the point's latitude φ, may be obtained from Somigliana's formula (Moritz, 1992; Torge, 2001):

$$\gamma_{ell} = \frac{a\gamma_e cos^2\varphi + b\gamma_p sin^2\varphi}{\left(a^2 cos^2\varphi + b^2 sin^2\varphi\right)^{1/2}} \tag{25}$$

where γ_e and γ_p are the normal gravity at the equator and the poles, respectively, and other parameters are as previously described.

Residual anomalies, with respect to the GGMs, may be computed without terrain effects as follows (Marotta and Vidotti, 2017a):

$$\Delta g = \Delta g_{fa} - \Delta g_{ggm}$$

The residual free air anomalies and geoidal heights are a measure of how well that model represents the low-medium spectral information in a given area. The smoother these quantities are, the more efficiently the harmonic model represents the low degree spectrum locally.

4. Results and discussion

All the 31 GGMs are subjected to external validation using GNSS-levelled points and observed free-air anomalies. Thereafter, some of the best performers are subjected further to internal validation using spectral analysis for the purpose of identifying the most optimum models for geoid modelling in Kenya. To minimize the effect of gross errors as well as systematic errors in the gravity data, the data were filtered such that a difference of less than 20 mGal was true between the gravity accelerations and the normal gravity computed at the terruloid

Table 6
Statistics of synthesized undulations from selected GGMs computed to their maximum degree (units are in metres).

Model	Max Degree	Min	Max	Mean	Std Dev.
SGG-UGM-2	2190	−29.304	−13.156	−19.702	6.529
XGM 2019e_2159	2190	−29.272	−13.165	−19.697	6.540
XGM 2019e	5540	−29.274	−13.164	−19.695	6.544
XGM2019	760	−29.271	−13.064	−19.680	6.563
ITSG-Grace2018s	200	−29.504	−12.769	−19.561	6.780
GOCO06s.	300	−29.424	−13.050	−19.574	6.643
GO_CONS_GCF_2_TIM_R6	300	−29.418	−13.051	−19.568	6.645
GO_CONS_GCF_2_DIR_R6	300	−29.484	−13.063	−19.593	6.675
IGGT_R1C	240	−29.563	−13.035	−19.580	6.854
Tongji-Grace02k	180	−29.133	−12.866	−19.137	6.632
SGG-UGM-1	2159	−29.287	−13.161	−19.724	6.541
GOSG01S	220	−29.871	−12.963	−19.590	6.831
IGGT_R1	240	−29.572	−13.224	−19.622	6.765
IfE_GOCE05s	250	−29.462	−13.105	−19.560	6.664
GO_CONS_GCF_2_SPW_R5	330	−29.437	−13.032	−19.648	6.662
XGM2016	719	−29.245	−13.070	−19.675	6.565
Tongji-Grace02s	180	−29.189	−12.723	−19.140	6.693
NULP-02s	250	−29.455	−12.926	−19.516	6.710
EIGEN-6C4	2190	−29.406	−13.142	−19.722	6.566
GO_CONS_GCF_2_DIR_R5	300	−29.508	−13.037	−19.630	6.672
GO_CONS_GCF_2_TIM_R4	250	−29.513	−13.045	−19.576	6.731
GO_CONS_GCF_2_TIM_R3	250	−29.435	−12.902	−19.499	6.710
GO_CONS_GCF_2_TIM_R2	250	−29.532	−12.959	−19.544	6.775
GOCO02s	250	−29.501	−12.978	−19.535	6.755
EGM2008	2190	−29.257	−13.131	−19.717	6.541
EIGEN-GL04C	360	−29.297	−12.924	−19.502	6.616
eigen-cg03c	360	−29.165	−12.775	−19.401	6.599
EIGEN-CHAMP03S	140	−28.346	−13.808	−18.780	6.391
EGM96	360	−29.327	−12.716	−19.589	6.609
EIGEN-2	140	−28.302	−14.504	−19.155	6.273
GEM10b	36	−26.938	−12.966	−19.545	5.126

point of each gravity station. The terruloid point of a gravity station is the point along the normal plumbline through the station, whose normal gravity potential is the same as the true potential of the gravity station. The threshold of 20mGal has been used by various researchers (Kiamehr, 2004; Sulaiman et al., 2013) and found to be suitable. The statistics of the final gravity data used are shown in Table 5.

4.1. External validation using observed data

Equations (3) and (4) were used to synthesize geoid heights and gravity anomalies from the selected GGMs at the GNSS-levelled points and the gravity stations, respectively. MATLAB functions, that are part of a geoid computation software which is at the developmental stage by the authors, were used to carry out the computations. The earth's geocentric gravitational constant (GM_E) was derived from the GGMs. In all GGMs, a value of $GM_E = 3.986004415e14$ was used, except for GEM10b which had $GM_E = 3.986004461e14$. The reference GM_0, the normal potential, U_0, the mean Earth radius R and the mean normal gravity γ were obtained from the reference ellipsoid. For the WGS84 ellipsoid (Kumar, 1993), $GM_E = 3.986004.418e14, U_0 = 62636851.7146, R = 6371008.771$, and $\gamma = 9.797643222$ m s^{-2}. The gravity potential of the geoid was set as $W_0 = 62636853.4$ m2s-2, which was adopted as a realization of the potential value for the International Height Reference System (IHRS) during the 2015 International Union of Geodesy and Geophysics (IUGG) General Assembly (Sánchez and Sideris, 2017).

4.1.1. Computation of zero-degree terms

The zero-degree terms for the geoid undulation and gravity anomalies were computed first for each GGM using equations (5) and (6) and the constants described above, and the results were added to the synthesized functionals. For the WGS84 ellipsoid, mean values of −0.1768m and −0.00074mGal were obtained for the geoid undulation and gravity anomalies, respectively, for all the GGMs, except for GEM10b. The values for the GEM10b were −0.1031m and 0.0106mGal, respectively for geoid undulation and gravity anomalies.

Table 7
Statistical results of the differences $N_{gnss} - N_{ggm}$ between the observed and synthesized geoid undulations at 55 GNSS/levelling benchmarks (units are in metres).

Model	Max Degree	Min	Max	Mean	Std Dev.
GO_CONS_GCF_2_DIR_R5	300	−1.654	0.746	−0.507	0.815
GO_CONS_GCF_2_SPW_R5	330	−1.677	0.775	−0.489	0.820
GOCO06s	300	−1.762	0.644	−0.562	0.830
XGM2016	719	−1.816	0.648	−0.461	0.831
XGM2019	760	−1.809	0.638	−0.456	0.831
GO_CONS_GCF_2_TIM_R6	300	−1.772	0.642	−0.569	0.832
ITSG-Grace2018s	200	−1.782	0.862	−0.575	0.835
EGM96	360	−1.819	0.568	−0.547	0.837
XGM 2019e	5540	−1.799	0.623	−0.441	0.838
SGG-UGM-2	2190	−1.790	0.640	−0.435	0.839
SGG-UGM-1	2159	−1.776	0.649	−0.413	0.839
XGM 2019e_2159	2190	−1.801	0.625	−0.440	0.840
GO_CONS_GCF_2_DIR_R6	300	−1.744	0.716	−0.544	0.842
IfE_GOCE05s	250	−1.772	0.662	−0.576	0.843
EIGEN-6C4	2190	−1.799	0.643	−0.414	0.851
EGM2008	2190	−1.817	0.719	−0.419	0.855
Tongji-Grace02k	180	−2.250	0.282	−1.000	0.858
NULP-02s	250	−1.930	0.684	−0.621	0.858
GO_CONS_GCF_2_TIM_R3	250	−1.960	0.666	−0.637	0.864
Tongji-Grace02s	180	−2.294	0.330	−0.997	0.873
GO_CONS_GCF_2_TIM_R4	250	−1.858	0.794	−0.560	0.887
GOCO02s	250	−1.927	0.792	−0.601	0.896
GO_CONS_GCF_2_TIM_R2	250	−1.939	0.829	−0.592	0.909
EIGEN-GL04C	360	−2.101	0.493	−0.634	0.915
eigen-cg03c	360	−2.161	0.443	−0.736	0.921
IGGT_R1	240	−1.786	0.922	−0.514	0.933
GOSG01S	220	−1.920	1.007	−0.547	0.946
IGGT_R1C	240	−1.828	1.038	−0.557	0.956
EIGEN-CHAMP03S	140	−2.512	1.127	−1.356	1.090
EIGEN-2	140	−2.258	1.819	−0.981	1.144
GEM10b	36	−4.034	3.479	−0.592	2.246

4.1.2. Comparison using GNSS-levelled points

Using the known ellipsoidal and orthometric heights of the GNSS-levelled stations, observed geoid heights were computed using equation (13), the statistics of which are shown in Table 2. Table 6 shows the statistics of the results of the synthesized undulations.

The differences between the observed and the synthesized geoid undulations were computed using equation (14), and the statistics of the results are given in Table 7. In the table, the GGMs are ranked in ascending order of the standard deviations obtained.

From the values given in Table 7, there is evidence of some bias between the geopotential of the zero-height surface of the Kenya vertical datum and the conventional value $W_0 = 62636856.00$ m^2/s^2, which is the equipotential surface specified by the International Earth Rotation Service (IERS) and was used in the development of the various GGMs over the Kenyan region. These discrepancies are likely due to long/medium-wavelength errors in the spherical harmonic coefficients (Kotsakis and Katsambalos, 2010).

In order to model the systematic errors, least-squares parametric fitting was carried out using the models discussed in section 3.5. The obtained residuals were added to the observations ($h - H$) and the results compared with the GNSS-level undulations. This improved the standard deviations as shown in Table 8.

Among the selected GGMs, the GO_CONS_GCF_2_DIR_R5 produced the lowest standard deviation of 0.815m of the difference between GNSS based and geopotential-based undulations. After removing the systematic errors, the standard deviation improved in all models, with the higher resolution GGMs performing better than lower resolution GGMs. Comparing the parametric models used, the seven-parametric model

Table 8
Standard deviations of the differences $N_{gnss} - N_{ggm}$ for geoid undulations at the 55 GNSS/levelling benchmarks, after the least-squares fitting using various parametric models (units are in metres).

Model	Nmax	Parametric Model (No. of parameters)			
		3	4	5	7
EGM2008	2190	0.78939	0.49801	0.41284	0.40888
SGG-UGM-1	2159	0.78005	0.50062	0.41458	0.40909
SGG-UGM-2	2190	0.78578	0.49613	0.41573	0.40975
EIGEN-6C4	2190	0.79153	0.49220	0.41566	0.41003
XGM 2019e	5540	0.77896	0.50382	0.42001	0.41310
XGM 2019e_2159	2190	0.78141	0.50590	0.42112	0.41419
XGM2019	760	0.76299	0.49841	0.42283	0.41638
XGM2016	719	0.76154	0.50391	0.42404	0.41768
EGM96	360	0.74404	0.47490	0.44532	0.42252
GO_CONS_GCF_2_DIR_R5	300	0.70443	0.52502	0.46225	0.44011
EIGEN-GL04C	360	0.83762	0.53720	0.48084	0.44050
eigen-cg03c	360	0.84196	0.52060	0.47010	0.44174
GO_CONS_GCF_2_SPW_R5	330	0.71583	0.53552	0.47031	0.44420
GOCO06s	300	0.74187	0.54477	0.48032	0.45134
GO_CONS_GCF_2_DIR_R6	300	0.73535	0.55033	0.48316	0.45256
GO_CONS_GCF_2_TIM_R6	300	0.74269	0.54815	0.48308	0.45363
ITSG-Grace2018s	200	0.61658	0.51737	0.46849	0.45973
IGGT_R1.gfc	240	0.77649	0.61486	0.51604	0.47027
IfE_GOCE05s	250	0.73879	0.56861	0.50201	0.47158
GO_CONS_GCF_2_TIM_R4	250	0.75377	0.56924	0.50071	0.47956
GO_CONS_GCF_2_TIM_R2	250	0.75212	0.56495	0.50030	0.48364
GOCO02s	250	0.74744	0.56750	0.50177	0.48444
IGGT_R1C	240	0.70714	0.60019	0.51266	0.48593
GO_CONS_GCF_2_TIM_R3	250	0.74159	0.55498	0.50348	0.48650
NULP-02s	250	0.73371	0.55453	0.50182	0.48662
GOSG01S.gfc	220	0.75788	0.55957	0.52236	0.49239
Tongji-Grace02s	180	0.74613	0.58095	0.52301	0.51199
Tongji-Grace02k	180	0.75815	0.60214	0.53927	0.51872
GEM10b	36	1.25034	0.98475	0.62548	0.56046
EIGEN-CHAMP03S	140	0.99405	0.89258	0.63623	0.57833
EIGEN-2	140	1.05484	1.00063	0.67912	0.58948

Table 9
Statistics of synthesized free-air anomalies for the selected GGMs computed to their maximum degree at 7456 stations (Units are in mGal).

Model	Max Degree	Min	Max	Mean	Std Dev.
SGG-UGM-2	2190	−57.963	70.577	−2.239	12.983
XGM 2019e_2159	2190	−56.149	76.934	−3.592	13.507
XGM 2019e	5540	−57.177	38.833	−4.196	12.730
XGM2019	760	−55.528	69.417	−1.894	16.533
ITSG-Grace2018s	200	−45.049	66.239	2.505	23.030
GOCO06s	300	−52.541	73.476	−0.186	21.015
GO_CONS_GCF_2_TIM_R6	300	−52.033	72.984	−0.113	20.943
GO_CONS_GCF_2_DIR_R6	300	−48.268	69.833	0.256	20.952
IGGT_R1C	240	−49.814	58.942	1.601	22.145
Tongji-Grace02k	180	−36.830	53.326	2.822	23.109
SGG-UGM-1	2159	−61.943	70.513	−2.187	12.946
GOSG01S	220	−50.480	58.145	1.714	21.961
IGGT_R1	240	−46.437	73.404	0.532	20.804
IfE_GOCE05s	250	−46.698	66.407	0.863	21.588
GO_CONS_GCF_2_SPW_R5	330	−54.138	72.022	0.159	20.926
XGM2016	719	−56.037	73.825	−1.817	16.673
Tongji-Grace02s	180	−33.072	57.145	3.587	23.512
NULP-02s	250	−48.103	61.647	1.687	21.843
EIGEN-6C4	2190	−62.450	70.952	−2.222	12.992
GO_CONS_GCF_2_DIR_R5	300	−47.071	70.837	0.345	21.738
GO_CONS_GCF_2_TIM_R4	250	−49.536	65.467	0.807	20.952
GO_CONS_GCF_2_TIM_R3	250	−50.202	63.297	1.520	21.686
GO_CONS_GCF_2_TIM_R2	250	−47.035	57.619	1.885	21.828
GOCO02s	250	−46.712	57.222	1.887	21.832
EGM2008	2190	−61.365	72.835	−2.049	13.134
EIGEN-GL04C	360	−52.004	81.709	1.767	21.656
eigen-cg03c	360	−52.187	78.400	2.127	21.691
EIGEN-CHAMP03S	140	−24.597	37.892	2.420	18.330
EGM96.gfc	360	−54.914	83.811	2.031	21.910
EIGEN-2	140	−25.242	35.534	2.257	14.842
GEM10b	36	−17.152	7.848	−0.154	6.281

Table 10
Statistics of residual free air anomalies over Kenya referred to the selected GGMs at 7456 points (Units are in mGal).

Model	Max Degree	Min	Max	Mean	Std Dev.
EIGEN-6C4	2190	−67.316	60.071	−2.141	6.892
SGG-UGM-1	2159	−66.877	59.563	−2.176	6.896
SGG-UGM-2	2190	−66.942	55.583	−2.124	6.954
EGM2008	2190	−69.200	58.986	−2.315	7.061
XGM 2019e	5540	−37.294	54.797	−0.167	7.174
XGM 2019e_2159	2190	−73.299	53.769	−0.771	8.683
GEM10b	36	−27.951	36.710	−4.209	10.636
XGM2019	760	−81.657	53.149	−2.469	12.075
XGM2016	719	−77.128	53.658	−2.546	12.289
EIGEN-2	140	−51.538	44.092	−6.621	14.080
EIGEN-CHAMP03S	140	−57.664	44.412	−6.783	16.204
GO_CONS_GCF_2_SPW_R5	330	−62.087	51.286	−4.522	16.902
GO_CONS_GCF_2_TIM_R6	300	−67.799	48.952	−4.250	17.055
GO_CONS_GCF_2_DIR_R6	300	−66.578	47.386	−4.620	17.067
GOCO06s	300	−67.596	49.559	−4.178	17.108
EIGEN-GL04C	360	−78.888	50.328	−6.130	17.241
GO_CONS_GCF_2_TIM_R4	250	−69.717	55.543	−5.171	17.308
eigen-cg03c	360	−77.940	48.726	−6.490	17.309
EGM96	360	−82.952	47.321	−6.394	17.321
IGGT_R1	240	−69.790	53.266	−4.895	17.394
GO_CONS_GCF_2_DIR_R5	300	−65.004	47.305	−4.708	17.713
IfE_GOCE05s	250	−70.414	52.207	−5.226	18.009
GO_CONS_GCF_2_TIM_R3	250	−67.151	53.702	−5.883	18.224
NULP-02s	250	−65.924	54.544	−6.050	18.307
GOCO02s	250	−68.900	52.950	−6.251	18.566
IGGT_R1C	240	−62.912	51.049	−5.964	18.577
GO_CONS_GCF_2_TIM_R2	250	−69.948	52.731	−6.248	18.591
GOSG01S	220	−70.511	53.336	−6.077	18.747
ITSG-Grace2018s	200	−67.519	56.674	−6.868	19.595
Tongji-Grace02k	180	−68.000	53.376	−7.186	19.607
Tongji-Grace02s	180	−66.744	49.454	−7.950	19.963

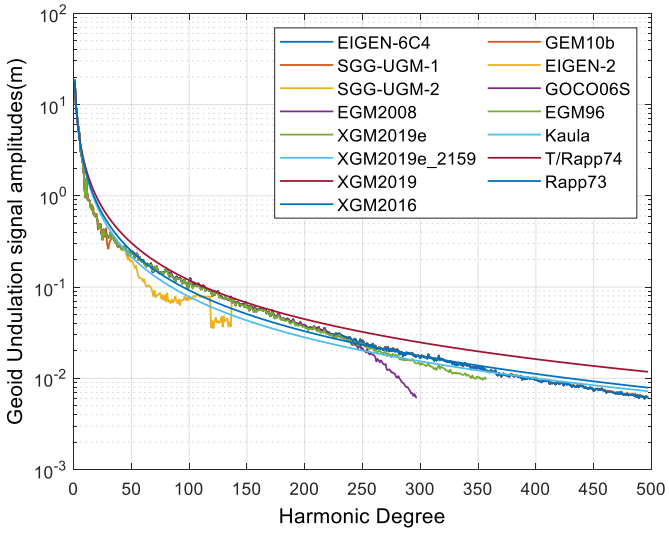

Fig. 2. Geoid undulation signal amplitudes.

produced smaller standard deviations for all GGMs, and therefore was used to rank the performance of the GGMs in terms of geoid heights. Overall, EGM2008 showed some slight advantage with a standard deviation of 40.888 cm, but SGG-UGM-1, SGG-UGM-2, EIGEN-6C4, XGM 2019e, XGM 2019e_2159, XGM2019 and XGM2016 performed well with a standard deviation of <42 cm. It is worth noting that EGM96 performed the best when the four-parametric model was used.

4.1.3. Comparison with free air anomalies

The free-air gravity anomalies have been synthesized from the geopotential models and compared with the observed free-air gravity

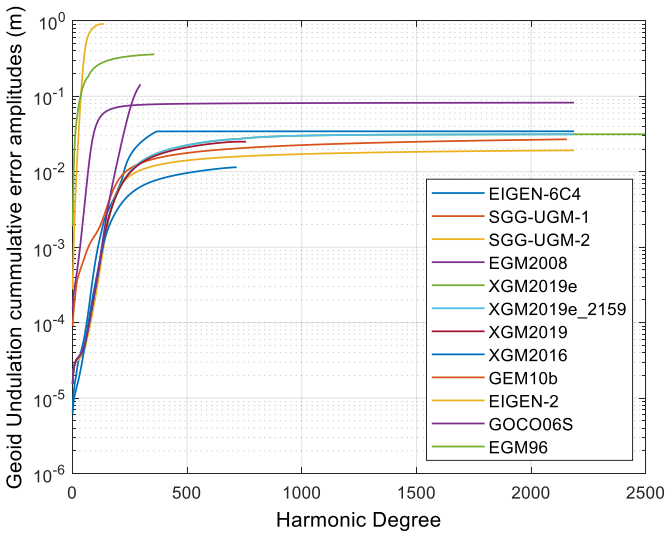

Fig. 3. Geoid undulation cumulative error amplitudes.

anomalies calculated at the gravity stations. Table 9 shows the statistics of the synthesized gravity anomalies. Residual anomalies were obtained after subtracting the synthesized anomalies from the observed anomalies. Table 10 shows the statistical results of the residual anomalies.

As can be observed from Table 10, the higher resolution GGMs outperformed the lower ones. EIGEN-6C4, SGG-UGM-1 and SGG-UGM-2 produced the best fit in terms of gravity anomalies in Kenya because of their low standard deviation of <7 mGal. The ranking of the performance of the GGMs is shown in the table. In the following section, the ten best performers in terms of both geoid undulations and gravity anomalies were chosen for spectral analysis.

4.2. Internal validation using spectral information

The spectral information for the best performing GGMs was compared using the procedures of section 3.4, up to a maximum degree of 500 for signal spectra and maximum degree for error spectra. The spectra of the signal, as well as the cumulative error for the selected models are depicted in Figs. 2 and 3, respectively, by degree in terms of geoid undulation. The global degree variance models of Kaula rule of thumb (Kaula, 1966), Tscherning and Rapp (1974), and Rapp (1973) for the decay of the fully normalized potential coefficients (see Table 4) are also shown.

From Fig. 2, it is shown that the geopotential models are generally close to one another and obey the global degree variance models of

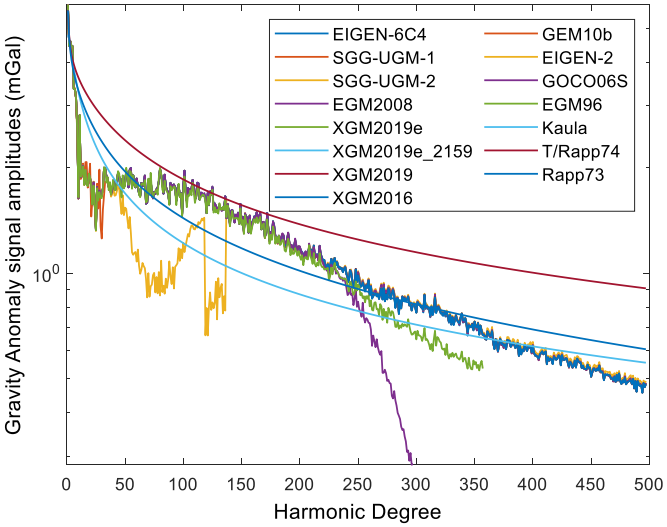

Fig. 4. Gravity anomaly signal amplitudes.

Table 11
RMSE of Geoid undulation signal amplitudes by wavelength (Units are in metres).

Model	Max Degree	Long 3 < N < 10	Intermediate 10 < N < 100	Short 100 < N < 1000	Very Short N > 1000	Total
EIGEN-6C4	2190	15.061	3.976	0.779	0.022	15.596
SGG-UGM-1	2159	15.060	3.976	0.777	0.022	15.596
SGG-UGM-2	2190	15.060	3.976	0.779	0.023	15.596
EGM2008	2190	15.061	3.976	0.777	0.022	15.596
XGM 2019e	2190	15.061	3.976	0.779	0.023	15.596
XGM 2019e_2159	2190	15.061	3.976	0.779	0.023	15.596
XGM2019	760	15.061	3.976	0.779	–	15.596
XGM2016	719	15.061	3.976	0.778	–	15.596
GEM10b	36	15.052	3.603	–	–	15.477
EIGEN-2	140	15.061	3.858	0.399	–	15.552
GOCO06S	300	15.061	3.976	0.750	–	15.595
EGM96	360	15.062	3.969	0.747	–	15.594

Table 12
RMSE of Geoid undulation error amplitudes by wavelength (Units are in metres).

Model	Max Degree	Long 3 < N < 10	Intermediate 10 < N < 100	Short 100 < N < 1000	Very Short N > 1000	Total
EIGEN-6C4	2190	0.000	0.001	0.034	0.002	0.034
SGG-UGM-1	2159	0.000	0.001	0.022	0.015	0.027
SGG-UGM-2	2190	0.000	0.000	0.017	0.009	0.019
EGM2008	2190	0.000	0.037	0.072	0.014	0.082
XGM 2019e	2190	0.000	0.000	0.030	0.009	0.031
XGM 2019e_2159	2190	0.000	0.000	0.030	0.009	0.031
XGM2019	760	0.000	0.000	0.025	–	0.025
XGM2016	719	0.000	0.000	0.011	–	0.011
GEM10b	36	NaN	NaN	–	–	NaN
EIGEN-2	140	0.002	0.841	0.343	–	0.908
GOCO06S	300	0.000	0.000	0.144	–	0.144
EGM96	360	0.018	0.241	0.266	–	0.359

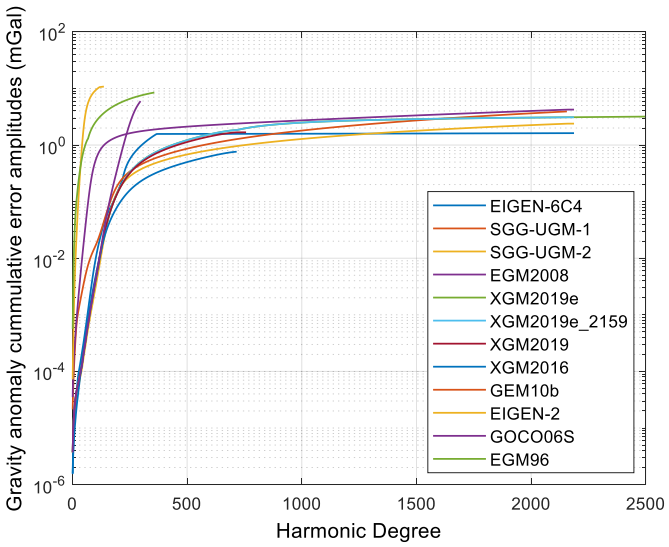

Fig. 5. Gravity anomaly cumulative error amplitudes of selected models.

Tscherning and Rapp (1974) and Rapp (1973) at the lower frequencies of less than 200°, which is equivalent to a linear half–wavelength of 100 km resolution or more. At higher degrees, the global degree variance models have more signal power than the actual gravity field. Further, it is shown that GOCO06S and EGM96 models lose power at about 230° and 240°, respectively. In Table 11, the RMSE of the geoid undulation signal is shown in terms of wavelength. Generally, all the higher resolution models (N > 700) have similar power, while the GEM10b model has the least power among the GGMs selected.

In Fig. 3, the cumulative errors in terms of the geoid undulation signal are plotted. Among the selected models, EIGEN-2 and EGM96 models have the highest cumulative error, while the XGM2016 model showed the lowest, which is also demonstrated in the last column of Table 12. Amongst the high-resolution models, EIGEN-6C4 showed the lowest geoid error. There was no error coefficient information in the GEM10b file.

In Figs. 4 and 5, the gravity anomaly signal and cumulative error amplitudes of the selected models are plotted. The RMSE of the signal and error spectra values by wavelength are tabulated in Table 13 and Table 14.

From Fig. 4 and Table 13, one can see that the high-resolution models have similar performance trends. Like in the geoid undulation signal, the GEM10 model has the lowest power, even at the lower frequencies, while the SGG-UGM-2 model has the highest. The GOCO06S and EGM96 models lose power at 230° and 240°. Among the global degree variance models, the T/Rapp74 and Rapp (1973) models seem to

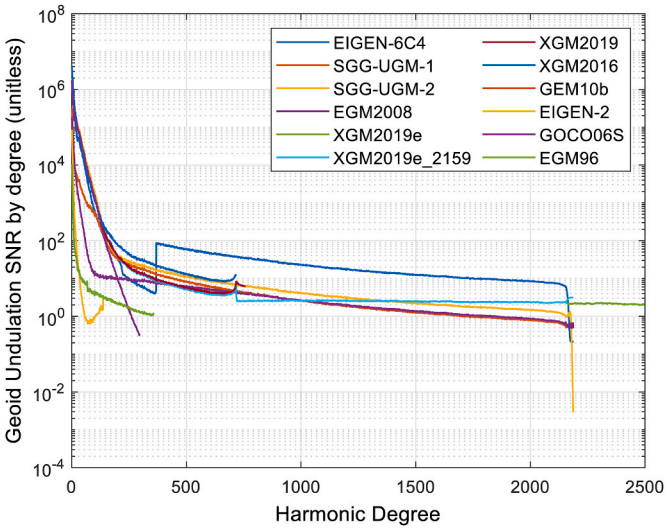

Fig. 6. Geoid undulation SNR of selected models.

Table 13
RMSE of Gravity anomaly signal amplitudes by wavelength (Units are in mGal).

Model	Max Degree	Long 3 < N < 10	Intermediate 10 < N < 100	Short 100 < N < 1000	Very Short N > 1000	Total
EIGEN-6C4	2190	10.618	17.152	21.133	4.521	29.563
SGG-UGM-1	2159	10.618	17.153	21.091	4.490	29.529
SGG-UGM-2	2190	10.618	17.152	21.244	4.615	29.657
EGM2008	2190	10.618	17.145	21.093	4.492	29.527
XGM 2019e	2190	10.618	17.152	21.110	4.621	29.562
XGM 2019e_2159	2190	10.618	17.152	21.110	4.600	29.559
XGM2019	760	10.618	17.152	20.669	–	28.882
XGM2016	719	10.618	17.152	20.658	–	28.874
GEM10b	36	10.603	9.160	–	–	14.011
EIGEN-2	140	10.618	13.789	7.063	–	18.782
GOCO06S	300	10.618	17.152	17.001	–	26.381
EGM96	360	10.619	17.086	17.743	–	26.824

Table 14
RMSE of Gravity anomaly error amplitudes by wavelength (Units are in mGal).

Model	Max Degree	Long 3 < N < 10	Intermediate 10 < N < 100	Short 100 < N < 1000	Very Short N > 1000	Total
EIGEN-6C4	2190	0.000	0.008	1.584	0.353	1.623
SGG-UGM-1	2159	0.000	0.016	1.797	3.485	3.922
SGG-UGM-2	2190	0.000	0.003	1.277	2.019	2.389
EGM2008	2190	0.000	0.492	2.680	3.233	4.229
XGM 2019e	2190	0.000	0.003	2.489	1.852	3.102
XGM 2019e_2159	2190	0.000	0.003	2.489	1.840	3.095
XGM2019	760	0.000	0.004	1.676	–	1.676
XGM2016	719	0.000	0.004	0.762	–	0.762
GEM10b	36	NaN	NaN	–	–	NaN
EIGEN-2	140	0.002	9.050	5.888	–	10.797
GOCO06S	300	0.000	0.004	5.965	–	5.965
EGM96	360	0.020	2.452	8.110	–	8.472

overestimate the power of the gravity anomaly signal more than the Kaula model.

From Fig. 5, it can be seen that the XGM2016 shows the lowest gravity anomaly cumulative error, followed by EIGEN-6C4, while XGM 2019, with the other high-resolution GGMs coming very close to one another. This is confirmed in Table 14, where the cumulative errors by wavelength are shown. EIGEN-2 and EGM96 models have the highest cumulative error.

In Fig. 6, the geoid signal power at different wavelengths is expressed in terms of SNR with the selected models. It can be seen that EIGEN-6C4 has the highest signal to noise ratio from about 360° upwards, followed by XMG_2019e_2159 and SGG-UGM-2. EIGEN-2 and EGM96 models have the lowest signal to noise ratios within the low wavelength spectra.

5. Conclusion

This study analyzed 31 global geopotential models that comprise the most recent and highest resolution available at the ICGEM. The analysis was done both spectrally and geometrically using local geodetic data spanning four regions of Kenya. The results reveal that all the high-resolution models selected in the study are capable of recovering geoid undulations to a reasonable accuracy. However, after removing gross and systematic errors, the EGM2008 showed some slight advantage with a standard deviation of 40.89 cm, followed by SGG-UGM-1, SGG-UGM-2, XGM 2019e, EIGEN-6C4, XGM 2019e, XGM 2019e_2159, XGM2019 and XGM 2016, with standard deviations of <42 cm. In terms of gravity anomalies, still the higher resolution GGMs performed better than low-resolution ones. EIGEN-6C4 performed best with a standard deviation of 6.892 mGal followed by SGG-UGM-1 and SGG-UGM-2 with standard deviations of <7 mGal. Spectral analysis was also performed on the ten ranking GGMs from the external evaluation process. EIGEN-2 and EGM96 models have the lowest signal power in terms of both geoid undulation and gravity anomalies, even within their spectral bands. The XGM2016 model produced the best error spectrum with the smallest cumulative geoid and gravity anomaly errors, followed by the SGG-UGM-2 model. In terms of signal to noise ratio, the EIGEN-2 and EGM96 models produced the lowest signal to noise ratios within the low wavelength spectra. XGM2016 produced the overall highest SNR, with the EIGEN-6C4 model producing the highest S/N ratio from degrees 360° upwards, followed by XMG_2019e_2159 and SGG-UGM-2. On the balance of performance in all the three areas of evaluation, the SGG-UGM-1 and SGG-UGM-2 models may jointly be ranked as the best for geoid modelling in Kenya.

Declaration of competing interest

The authors declare that they have no known competing financial interests or personal relationships that could have appeared to influence the work reported in this paper.

Acknowledgement

The authors are very grateful to Survey of Kenya for supplying the GNSS-levelling data and the Bureau Gravimetrique International (BGI) for supplying the gravity data that was used in this study. This project is funded by the Ministry of Higher Education (MOHE) under the Fundamental Research Grant Scheme (FRGS) Fund, Reference Code: FRGS/1/2020/WAB07/UTM/02/3 (UTM Vote Number: R.J130000.7852.5F304).

References

Ågren, J., 2004. Regional Geoid Determination Methods for the Era of Satellite Gravimetry:Numerical Investigations Using Synthetic Earth Gravity Models. PhD, Dissertation. Royal Institute of Technology, Stolkholm, Sweden.

Gachari, M.K., Olliver, J.G., 1986. The detailed gravimetric geoid of Kenya. Surv. Rev. 28 (221), 365–371. https://doi.org/10.1179/sre.1986.28.221.365.

Ghilani, C.D., Wolf, P.R., 2006. Adjustment Computations: Spatial Data Analysis. John Wiley & Sons, Inc.

Goyal, R., Dikshit, O., Balasubramania, N., 2018. Evaluation of global geopotential models: a case study for India. Surv. Rev. 1–11. https://doi.org/10.1080/00396265.2018.1468537.

Heiskanen, W., Moritz, H., 1967. In: Gilluly, J., Woodford, A.O. (Eds.), Physical Geodesy. W H Freeman and Company, San Francisco and London.

Ince, E.S., et al., 2019. ICGEM- 15 years of successful collection and distribution of global gravitational models, associated services and future plans. Earth Syst. Sci. Data Discuss. 1–61. https://doi.org/10.5194/essd-2019-17.

Ismail, M.K., et al., 2018. Establishment of new fitted geoid model in Universiti teknologi Malaysia. Int. Archiv. Photogrammetry, Rem. Sens. Spatial. Info. Sci-ISPRS Archives. 42 (4/W9), 27–33. https://doi.org/10.5194/isprs-archives-XLII-4-W9-27-2018.

Kaula, W.M., 1966. In: Gordon, J.F., MacDonald (Eds.), Theory of Satellite Geodesy. London: Blaisdell Publishing Company, Waltham, Massachusetts. Toronto.

Kearsley, A.H.W., Holloway, R.D., 1989. Tests on geopotential models in the Australian region. Aust. J. Geodes. Photogram. Survey 50, 1–17.

Kiamehr, R., 2004. 'an Optimum Local Geoid Model for Iran Based on the Least-Squares Modification of Stokes'S Formula', ncc.org.Ir, (2004), pp. 1–11. Available at: http://www.ncc.org.ir/_DouranPortal/Documents/r-kiamehr.pdf.

Kirby, J., Featherstone, W., 1997. A Study of Zero-and first-degree terms in geopotential models over Australia. Geomat. Res. Australia 66, 93–108.

Kotsakis, C., Katsambalos, K., 2010. Quality analysis of global geopotential models at 1542 GPS/levelling benchmarks over the Hellenic mainland. Surv. Rev. 42 (318), 327–344. https://doi.org/10.1179/003962610X12747001420500.

Kotsakis, C., Sideris, M.G., 1999. On the adjustment of combined GPS/levelling/geoid networks. J. Geodes. 73 (8), 412–421. https://doi.org/10.1007/s001900050261.

Kumar, M., 1993. World Geodetic System 1984: a Reference Frame for Global Mapping, Charting, and Geodetic Applications. Surveying & Land Information Systems.

Marotta, G.S., Vidotti, R.M., 2017a. Development of a local geoid model at the federal district, Brazil, patch by the remove- compute-restore technique, following helmert's condensation method. Bol. Ciências Geodésicas 23 (3), 520–538. https://doi.org/10.1590/S1982-21702017000300035.

Marotta, G.S., Vidotti, R.M., 2017b. Development OF a local geoid model at the federal district, Brazil, patch BY the remove- compute-restore technique, following HELMERT'S condensation method. Bol. Ciências Geodésicas 23 (3), 520–538. https://doi.org/10.1590/S1982-21702017000300035.

McCubbine, J., et al., 2018. Gsolve, a Python Computer Program with a Graphical User Interface to Transform Relative Gravity Survey Measurements to Absolute Gravity Values and Gravity Anomalies, vol. 7. *SoftwareX*. Elsevier B.V., pp. 129–137. https://doi.org/10.1016/j.softx.2018.04.003

Moritz, H., 1992. Geodetic reference system 1980. Bull. Geod. 54 (3), 395–405. https://doi.org/10.1007/BF02521480.

Odera, P.A., 2016. Assessment of EGM2008 using GPS/levelling and free-air gravity anomalies over Nairobi County and its environs. S. Afr. J. Geol. 5 (1), 17. https://doi.org/10.4314/sajg.v5i1.2.

Odera, P.A., 2020. Evaluation of the recent high-degree combined global gravity-field models for geoid modelling over Kenya. Geodesy Cartogr. 46 (2), 48–54. https://doi.org/10.3846/gac.2020.10453.

Rapp, R.H., 1973. Geoid information by wavelength (1946-1975). Bull. Geod. 110 (1), 405–411. https://doi.org/10.1007/BF02521950.

Rapp, R.H., 1974. Comparison of the Potential Coefficient Models of the Standard Earth (II and III) and the GEM 5 and GEM 6', (1), pp. 279–287.

Rapp, R.H., et al., 1991. Consideration of permanent tidal deformation in the orbit determination and data analysis for the TOPEX/POSEIDON mission. NASA Tech. Memorand., 100775, 1(January 1991).

Sánchez, L., Sideris, M.G., 2017. Vertical datum unification for the international height reference system (IHRS). Geophys. J. Int. 209 (2), 570–586. https://doi.org/10.1093/gji/ggx025.

Searle, R.C., 1970. A catalogue of gravity data from Kenya. Geophys. J. Int. (October) https://doi.org/10.1111/j.1365-246X.1970.tb00159.x.

Setan, H., Singh, R., 2001. Deformation analysis of a geodetic monitoring network. Geomatica 55 (3), 333–346. https://doi.org/10.1080/09715010.2013.860733.

Sideris, M.G., 2011. Geoid Determination , Theory and Principles. Encyclopedia of Earth Sciences Series, pp. 356–362. https://doi.org/10.1029/2007GL030356.Fowler. Part 5(January 2011).

Sjöberg, L.E., Bagherbandi, M., 2017. Gravity Inversion and Integration: Theory and Applications in Geodesy and Geophysics. Springer International Publishing, Berlin. https://doi.org/10.1007/978-3-319-50298-4.

Sulaiman, S.A.H., et al., 2013. Cross validation approach in qualification of observed gravity data. In: Proceedings - 2013 IEEE 4th Control and System Graduate Research Colloquium, ICSGRC 2013, (August), pp. 168–171. https://doi.org/10.1109/ICSGRC.2013.6653297.

Swain, C.J., Khan, M.A., 1978. A catalogue of gravity measurements in Kenya. Geophys. J. Int. 53 (2), 427–429.

Torge, W., 2001. Geodesy, third ed. Walter de Gruyter, Berlin, New york. https://doi.org/10.1515/9783110879957.

Tscherning, C.C., Rapp, R.H., 1974. Closed Covariance Expressions for Gravity Anomalies, Geoid Undulations, and Deflections of the Vertical Implied by Anomaly Degree Variance Models. Report no. 208. Dept. of Geodetic Science, The Ohio State University, Columbus.

Tsoulis, D., et al., 2011. Spectral analysis and interpretation of current satellite-only Earth gravity models by incorporating global terrain and crustal data. *ESA*. Thesaloniki.

Tziavos, I.N., et al., 2015. Validation of GOCE/GRACE Satellite Only and Combined Global Geopotential Models over Greece in the Frame of the GOCESeaComb Project. International Association of Geodesy Symposia, pp. 145–153.

Ustun, A., Abbak, R.A., 2010. On global and regional spectral evaluation of global geopotential models. J. Geophys. Eng. 7 (4), 369–379. https://doi.org/10.1088/1742-2132/7/4/003.

Wang, Y.M., 2012. On the omission errors due to limited grid size in geoid computations. In: Sneeuw, N., et al. (Eds.), VII Hotine-Marussi Symposium on Mathematical Geodesy. International Association of Geodesy Symposia, vol. 137. Springer Berlin Heidelberg, Berlin, Heidelberg, pp. 221–226. https://doi.org/10.1007/978-3-642-22078-4_33.

Zhang, P., et al., 2020. Estimation of vertical datum parameters using the gbvp approach based on the combined global geopotential models. Rem. Sens. 12 (24), 1–23. https://doi.org/10.3390/rs12244137.